J Solid State Electrochem (2011) 15:811–819
DOI 10.1007/s10008-010-1154-1

ORIGINAL PAPER

Layer-by-layer self-assembly and electrocatalytic properties of poly(ethylenimine)-silicotungstate multilayer composite films

Diana M. Fernandes · Christopher M. A. Brett · Ana M. V. Cavaleiro

Received: 18 June 2010 / Revised: 22 July 2010 / Accepted: 23 July 2010 / Published online: 6 August 2010

Abstract Hybrid multilayer films composed of poly (ethylenimine) and the Keggin-type polyoxometalates $[SiW_{11}O_{39}]^{8-}$ (SiW_{11}) and $[SiW_{11}Co^{II}(H_2O)O_{39}]^{6-}$ ($SiW_{11}Co$) were prepared on glassy carbon electrodes by layer-by-layer self-assembly, and were characterized by cyclic voltammetry and scanning electron microscopy. UV-vis absorption spectroscopy of films deposited on quartz slides was used to monitor film growth, showing that the absorbance values at characteristic wavelengths of the multilayer films increase almost linearly with the number of bilayers. Cyclic voltammetry indicates that the electrochemical properties of the polyoxometalates are maintained in the multilayer films, and that the first tungsten reduction process for immobilized SiW_{11} and $SiW_{11}Co$ is a surface-confined process. Electron transfer to $\left[Fe(CN)_6\right]^{3-/4-}$ and $\left[Ru(NH_3)_6\right]^{3+/2+}$ as electrochemical probes was also investigated by cyclic voltammetry. The $(PEI/SiW_{11}Co)_n$ multilayer films showed excellent electrocatalytic reduction properties towards nitrite, bromate and iodate.

Keywords Keggin-type silicotungstates · Polyoxometalates · Glassy carbon-modified electrodes · Layer-by-layer (LBL) self-assembly

This work is dedicated to the memory of Professor Helena Maria Carapuça.

D. M. Fernandes · A. M. V. Cavaleiro (✉)
Department of Chemistry/CICECO, University of Aveiro,
3810-193 Aveiro, Portugal
e-mail: anacavaleiro@ua.pt

C. M. A. Brett
Department of Chemistry, Faculty of Science and Technology,
University of Coimbra,
3004-535 Coimbra, Portugal

Introduction

Polyoxometalates (POMs) constitute a wide class of molecular metal-oxygen clusters with remarkable chemical, structural, and electronic versatility, which play an important role in areas as catalysis [1–3], medicine [4] and materials science [5–7]. Many POMs have been extensively applied in the field of chemically modified electrodes, due to their well-defined structure, good thermal and redox stability, electrocatalytic properties and ability to undergo very fast and reversible multi-electron electrochemical reactions [8, 9]. However, many practical applications of POMs depend on the fabrication of POM-based devices with specific molecular architectures. Many techniques have been developed to fabricate composite materials that incorporate POMs, namely Langmuir–Blodgett deposition [10], sol–gel processing [11] and electrodeposition [12, 13]. In recent years, layer-by-layer (LbL) assembly has proved to be a promising technique for fabricating uniform and ultrathin films, carried out by the alternate immersion of a solid substrate into solutions containing the chosen oppositely charged species [14–17]. Functional components, including transition metal complexes, cationic surfactants and polycations or polyanions, amongst others, can be self-assembled in an orderly manner into multilayer films of well-defined thickness, composition and structure [16]. Many examples of the application of the method to the preparation of POM materials have been reported [18, 19]. A variety of substrates of various shapes and sizes have been successfully employed as supports for the deposition of LbL films [15, 20].

We have been exploiting the potentialities of electrode modification by transition metal-substituted Keggin-type phospho- and silicotungstates [21–24]. These POMs are attrative as electrocatalysts, presenting different types of

potentially active sites, the performance depending on the substituting transition metal [2, 3]. Their use in electrocatalysis and in sensors [3, 8] has much to still be explored. The study described here concerns electrostatically assembled films with positively charged poly(ethylenimine) (PEI) and Keggin-type POM anions.

Keggin polyoxometalates, $[XM_{12}O_{40}]^{m-}$, where M=W or Mo and X=P, Si, are amongst the most used POMs in the preparation of films and/or functionalized electrodes [19, 25–28]. However, the related mono-lacunary and metal-substituted anions, ($[XM_{11}O_{39}]^{m-}$ and $[XM_{11}M'(H_2O)O_{39}]^{p-}$, respectively) have been much less studied. Only a few examples can be found of the use of transition metal monosubstituted Keggin polyoxotungstate anions in films prepared by the layer-by-layer self-assembly method [21, 29, 30]. Various films formed through the association of cationic PEI (on top of anchorage layers) and Keggin-type and related polyoxotungstates have been prepared, namely with $[BW_{12}O_{40}]^{5-}$ [31], $[SiW_{12}O_{40}]^{4-}$ [32], $[SiVW_{11}O_{40}]^{5-}$ [33], $[Eu(SiW_{10}VO_{39})_2]^{15-}$ [34], $[Co_4(H_2O)_2(PW_9O_{34})_2]^{10-}$ [35], $[PW_{11}Fe(H_2O)O_{39}]^{4-}$, $[SiW_{11}Fe(H_2O)O_{39}]^{5-}$ [21], and have been used for different purposes (electrocatalysis, luminescence and photochromism).

In the present work, stable ultrathin multilayer films by LbL self-assembly, incorporating lacunary or cobalt-substituted tungstosilicates, $[SiW_{11}O_{39}]^{8-}$ (SiW_{11}) or $[SiW_{11}Co^{II}(H_2O)O_{39}]^{6-}$ ($SiW_{11}Co$), respectively, and PEI have been prepared. Growth of the multilayer films on a quartz slide was monitored by UV-vis absorption spectroscopy. The electrochemical behaviour of the immobilized polyoxoanions and in the presence of $[Fe(CN)_6]^{3-/4-}$ and $[Ru(NH_3)_6]^{3+/2+}$ as electroactive species was investigated by cyclic voltammetry. The surface morphology of the films on glassy carbon electrodes was examined by scanning electron microscopy (SEM).

Additionally, the possible application of $(PEI/SiW_{11}Co)_n$ modified electrodes to the analytical determination of nitrite, bromate and iodate was tested. The determination of all three of these anions is important, due to their environmental and health implications. Nitrite is commonly used as a preservative in meat and fish. The potential risks of its use are balanced against the unique protective effect against toxin-forming bacteria [36]. Bromate (BrO_3^-) is generally found in drinking water samples as a by-product of ozone disinfection, and is widely used as a food additive [37]. Potassium iodate has been extensively used for iodination of commercial table salts. Therefore, the importance of improved analytical methods for determination of iodate and bromate has received considerable attention [38]. Nitrites have been commonly used as a model analyte for assessing the electrocatalytic properties of Keggin-type polyoxometalates [2, 8]. Some examples of the use of modified electrodes with these polyoxometalates for the determination of iodate and bromate can be found in the literature, namely for polyoxotungstates [39–42], although these analytes are less used than nitrite.

Experimental section

Reagents and solutions

The potassium salts $K_8[SiW_{11}O_{39}]\cdot 13H_2O$ and $K_6[SiW_{11}Co(H_2O)O_{39}]\cdot 12H_2O$ were prepared as described in the literature [43, 44]. Both compounds were characterized by thermal and elemental analysis, infrared spectroscopy and powder X-ray diffraction, and the results were in agreement with previously published values [44].

Poly(ethylenimine) (MW=50,000–100,000; 30 wt.% aqueous solution; branched, consisting of tertiary, secondary and primary amino groups in the ratio of 25/50/25, respectively) was purchased from Polysciences Europe GmbH and was used without further treatment. Sodium chloride (Merck), potassium chloride (Merck), acetic acid (Pronalab), sodium acetate (Carlo Erba), potassium ferricyanide (Merck), hexaammineruthenium(III) chloride (Aldrich), sodium nitrite (Merck), sodium bromate (Sigma-Aldrich), potassium iodate (Sigma-Aldrich) and other reagents were analytically graded and used as received.

Electrolyte solutions for voltammetry were prepared using ultra-pure water (resistivity 18.2 MΩ cm at 25 °C, Direct-Q 3 UV system, Millipore). Solutions with pH 4.0 used for electrochemical studies were prepared by mixing appropriate amounts of CH_3COOH (0.1 M) and $NaCH_3COO$ (0.1 M) solutions. Solutions of redox probes (1.0 mM) were prepared dissolving the appropriate amounts of $K_3[Fe(CN)_6]$ and $[Ru(NH_3)_6]Cl_3$ in 1 M KCl.

The solutions used for multilayer film formation were used immediately after their preparation and degassed with pure nitrogen for at least 10 min.

Instrumentation and methods

UV-vis absorption spectroscopy of the SiW_{11} and $SiW_{11}Co$ solutions was performed using a quartz cell with 0.4 cm path length in a Jasco V-560 UV-visible spectrophotometer. A set of seven solutions of each compound (0.001–0.05 mM) in acetate buffer (pH 4.0) was used to determine the isotropic molar absorption coefficient. UV-vis absorption spectra of multilayer films were recorded on quartz slides.

Electrochemical experiments were carried out on a computer controlled potentiostat (PGSTAT-12/GPES software from Autolab/Ecochemie, The Netherlands). A conventional three-electrode cell was used. The auxiliary and reference electrodes were platinum wire (7.5 cm, BAS, MW-1032) and Ag/AgCl (sat. KCl; BAS, MF-2052),

respectively. The working electrode was a glassy carbon disc, GCE, (3 mm diameter, BAS, MF-2012), bare or surface-modified with the LbL films. A combined glass electrode (Hanna Instruments HI 1230) connected to an Inolab pH level 1 pH meter was used for the pH measurements. All measurements were made at room temperature (~20ºC).

Scanning electron microscopy was conducted on an Analytical FE-SEM SU-70 Hitachi, UHR 1.0 nm/15 kV (1.6 nm/1 kV). Elemental analysis, powder X-ray diffraction, thermogravimetric and FTIR studies were performed as indicated previously [45].

Preparation of self-assembled $(PEI/POM)_n$ films

Films were prepared on glassy carbon electrodes and on quartz slides. Prior to coating, the GCE was conditioned by a polishing/cleaning procedure. The GCE was polished with 1.0-μm diamond polishing compound (Metadi II, Buehler) followed by aluminium oxide of particle size 0.3 μm (Buehler–Masterprep) on a microcloth polishing pad (BAS Bioanalytical Systems Inc.), then the electrode was rinsed with ultra-pure water and finally sonicated, for 5 min, in an ultrasonic bath (Branson 2510). Quartz slides were cleaned by placing them in a H_2SO_4/H_2O_2 (3:1) (*v*/*v*) hot bath (~80º C) for 40 min and then in a $H_2O/H_2O_2/NH_3$ (5:1:1) (*v*/*v*/*v*) hot bath (~80ºC) for another 40 min. The cleaned quartz slides were then rinsed with ultra-pure water and dried under a stream of pure nitrogen.

After the cleaning step, the GCE or quartz slides were immersed in a 5 mg/mL PEI solution (in pH=4.0 acetate buffer) for 20 min. The GCE was then immersed in a 0.3 mM POM solution (in pH=4.0 acetate buffer) for 20 min. This process was repeated until the desired number of layers was obtained. Water rinsing and nitrogen drying steps were performed after each immersion.

Results and discussion

Multilayer films were assembled through the alternate adsorption of cationic PEI and of the α−isomers of the Keggin-type polyoxoanions $[SiW_{11}O_{39}]^{8-}$ and $[SiW_{11}Co(H_2O)O_{39}]^{6-}$. The deposition was performed on quartz slides and on glassy carbon, in pH 4.0 aqueous solutions of the POM potassium salts and of branched PEI.

Characterization of multilayer $(PEI/POM)_n$ films deposited on quartz slides

UV-vis spectroscopy was used to monitor the growth process of the multilayer films deposited on quartz slides. Figure 1 shows UV-vis spectra after the deposition of each

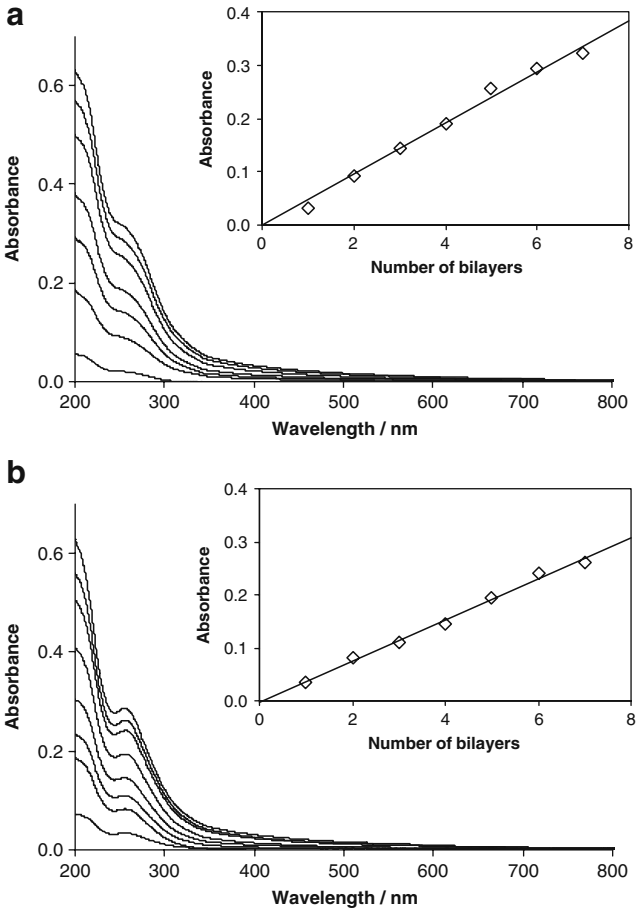

Fig. 1 UV-vis absorption spectra of **a** $(PEI/SiW_{11})_n$ and **b** $(PEI/SiW_{11}Co)_n$ multilayers for n=0–7 adsorbed on a quartz slide. The insets in **a** and **b** show the absorbance at **a** 248 nm and **b** 254 nm, as a function of n

bilayer of $(PEI/SiW_{11})_n$ and $(PEI/SiW_{11}Co)_n$. The spectra present two absorption bands in the ultraviolet region; the absorbance increased linearly with the number of bilayers, and the positions and shape of the bands did not change during multilayer construction. PEI does not absorb above 200 nm and the films exhibit the two characteristic bands of heteropolyanions with the Keggin structure at around 195 and 250 nm, both associated with O→W charge transfer transitions [46]. The spectra obtained are identical to those of the POMs in aqueous solution, but the low intensity *d*-*d* bands of cobalt(II), at around 550 nm [44], were not discernible. The absorption bands at 248 nm (SiW_{11}) and 254 nm ($SiW_{11}Co$) were chosen to monitor film growth. The insets in Fig. 1 show that the absorbance increases almost linearly with the number of deposited layers, suggesting that the quantity of polyoxometalate deposited per bilayer was approximately the same up to seven bilayers, both for SiW_{11} and $SiW_{11}Co$. With a further increase in the number of bilayers, the absorbance increases less, reaching a plateau.

The surface coverage per layer, Γ, can be estimated from the spectra of the multilayers, according to the Beer–Lambert law, $\Gamma = A_\lambda/2m\varepsilon_\lambda$, where A_λ is the absorbance at the specified wavelength, m is the number of layers and ε_λ is the isotropic molar absorption coefficient ($M^{-1}cm^{-1}$) [15]. In aqueous solution (acetate buffer, pH 4.0), the isotropic molar absorption coefficients for SiW_{11} and for $SiW_{11}Co$ are $\varepsilon_{248} = 7.66 \times 10^4 M^{-1}cm^{-1}$ and $\varepsilon_{254} = 7.27 \times 10^4 M^{-1}cm^{-1}$, respectively. This leads to values of the surface coverage of 2.88×10^{-10} mol cm^{-2} for SiW_{11} and 2.63×10^{-10} mol cm^{-2} for $SiW_{11}Co$ for 20 min deposition time. These values are in agreement with previous results obtained by us for $PW_{11}Fe$ and $SiW_{11}Fe$ [21].

Scanning electron microscopy characterization

The morphology of the films deposited on glassy carbon was examined by SEM. Figure 2 shows representative images after the adsorption of two bilayers of (PEI/$SiW_{11}Co$) at different magnifications. The surface is completely covered by the film—the considerable number of cracks present (Fig. 2a) can be attributed partly to the effect of the vacuum in the SEM chamber and also, to a greater extent, to the high-energy beam (on increasing the magnification, cracks were formed in places where they did not exist previously). The higher magnification (Fig. 2b) reveals the presence of a high density of irregular-shaped domains of small nanometre dimensions underneath these cracks. The features of the SEM images were the same for larger numbers of bilayers. The results for SiW_{11} are very similar and so are not shown.

Voltammetric behaviour of multilayer films

Cyclic voltammograms of the lacunary SiW_{11} anion and of the metal-substituted $SiW_{11}Co$ in aqueous acidic solutions show two reversible or quasi-reversible two-electron waves at negative potentials, corresponding to the reduction of the tungsten atoms [12, 23, 47]. The voltammetric features of the films on GCE were also studied in aqueous acid solution, since α-Keggin silicotungstates are generally unstable in neutral and basic solutions.

Figure 3a shows representative examples of cyclic voltammograms obtained for single (PEI/POM) bilayers at different scan rates in pH 4.0 acetate buffer solution. Since PEI is not electroactive, its presence is not reflected in the cyclic voltammograms. Under the conditions used, two quasi-reversible two-electron waves were observed with reduction peaks at −714 and −885 mV for $SiW_{11}Co$ and at −711 and −876 mV vs. Ag/AgCl for SiW_{11} (Table 1), which demonstrates that the electrochemical behaviour of the two POM anions studied is maintained in the multilayer films. These redox peaks are attributed to two consecutive two-electron reduction processes occurring at four of the tungsten atoms ($W^{VI} \rightarrow W^{V}$), corresponding to a four-electron global reduction. The reduction/oxidation peak of the substituting metal ($Co^{III/II}$) was not observed because cobalt is not electroactive within the potential window used from −1.0 to 0.5 V. In the experimental timescale employed (scan rates in the range 15 to 300 mV s^{-1} for both types of (PEI/POM) multilayer film, the values of peak potential changed only slightly with scan rate, and the ratio of anodic to cathodic peak currents was close to 1.

The cathodic and anodic peak currents of the first W wave were directly proportional to the scan rate, which indicates a surface-confined process [48]. This is consistent with early findings for $[SiW_{11}Ni(H_2O)O_{39}]^{6-}$ deposited on a cysteamine modified gold electrode [39], $[PW_{11}Fe(H_2O)O_{39}]^{4-}$, $[SiW_{11}Fe(H_2O)O_{39}]^{5-}$ [21] and for the mixed anion $[SiVW_{11}O_{40}]^{5-}$ [33]. In addition, the anodic/cathodic peak-to-peak separation (ΔE_p) for the tungsten waves was ca. 30–50 mV instead of zero, expected for a reversible surface process, so there are kinetic or thermodynamic (due to the film thickness) constraints.

Table 1 presents voltammetric data for the immobilized POMs, where E_{pc} and E_{pa} are the cathodic and anodic peak potentials. The potentials for the first tungsten process at the SiW_{11} modified electrode are almost 70 mV more

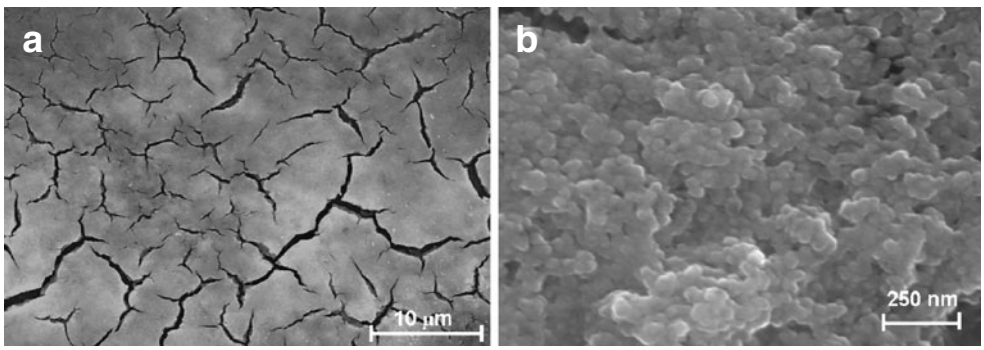

Fig. 2 Representative SEM micrographs of $(PEI/SiW_{11}Co)_2$ films on a glassy carbon electrode at different magnifications: **a** ×2,500 and **b** × 80,000

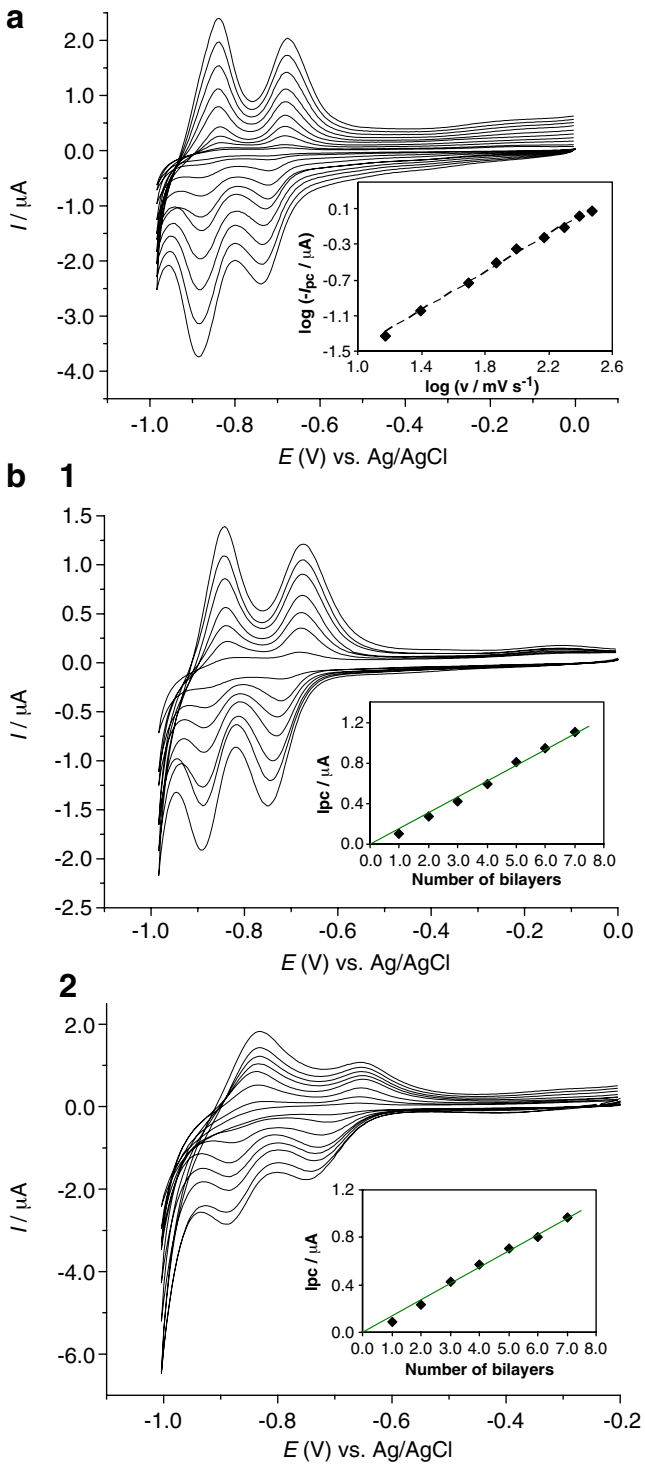

Fig. 3 Cyclic voltammograms in $CH_3COOH/NaCH_3COO$ buffer solution (pH 4.0) for **a** $(PEI/SiW_{11}Co)_1$ bilayer films at scan rates from 15 to 300 mVs^{-1}, **b** $(PEI/SiW_{11}Co)_n$ and $(PEI/SiW_{11})_n$ multilayer films in $CH_3COOH/NaCH_3COO$ buffer solution (pH 4.0) for n=1–7, v=50 mVs^{-1}

negative than the corresponding polyoxoanion in aqueous solution (E_{pc}=−643 mV at pH=4.0, H_2SO_4/Na_2SO_4 buffer). However, for $SiW_{11}Co$ the potentials are similar (E_{pc}= −730 mV at pH=4.0, same buffer). In aqueous solution, for the metal substituted POMs the potentials of the first tungsten reduction peak are shifted towards more negative values compared with those of the lacunary anion. However, when they are immobilized there are no changes of peak potential values, in agreement with reported data [23, 47]

Cyclic voltammograms for $(PEI/SiW_{11}Co)_n$ and $(PEI/SiW_{11})_n$ multilayer films with different numbers of layers are presented in Fig. 3b. In both cases, the cathodic peak potentials shift to more negative values by approximately 20 mV for $SiW_{11}Co$ and 30 mV for SiW_{11} and the anodic peak potentials shift slightly to more positive values with an increase in the number of layers, leading to a variation of the mid-point potential of about 20 mV. Usually, the build-up of charge due to reduction of POMs is compensated by protonation of the anions. The observed shift to more negative potentials with respect to aqueous solution is possibly due to the difficulty of POM charge compensation in the polymer environment [19, 49]. Plots of peak current vs. the number of bilayers (n), show linear growth up to n= 7 for both $SiW_{11}Co$ and SiW_{11}. Above these numbers of bilayers, peak currents begin to show a negative deviation from linearity, which can be ascribed to effects of film resistance, i.e. difficulty of transferring electrons through the film to the electrode substrate. Although the peaks for $(PEI/SiW_{11})_n$ multilayer films are not so well defined as for $(PEI/SiW_{11}Co)_n$, they appear at the expected potentials and the system exhibits the same characteristics.

Surface coverage can be calculated from cyclic voltammetry according to the equation $\Gamma = \left(4I_{pa}RT\right)/(n^2F^2\nu A)$ where I_{pa} is the anodic peak current (ampere), n is the number of electrons transferred (2 in this case), ν is the scan rate (Vs^{-1}), A is the geometric area of the electrode (0.0725 cm^2), R is the gas constant, T is the temperature (298 K) and F is the Faraday constant [50]. Peak currents were plotted against scan rate (10 to 300 mVs^{-1}) and the value of I_{pa}/v obtained was used to calculate the surface coverage. This led to a surface coverage of 1.50×10^{-11} mol cm^{-2} for SiW_{11} and 1.82×10^{-11} $molcm^{-2}$ for $SiW_{11}Co$. Comparing these values to the ones obtained for $PW_{11}Fe$-and $SiW_{11}Fe$-modified electrodes [21] with slightly different deposition conditions, these values correspond to sub-monolayer coverage. The surface coverages estimated by UV-visible spectroscopy are significantly different from these values but are calculated assuming that the molar absorption coefficients of the polyoxometalates are the same in solution and in the films, which is not certain. Also diffuse scattering is expected due to the heterogeneity of the surface: these scattering losses would give rise to a lower intensity of

Table 1 Cyclic voltammetric data for the deposited PEI/POM films on the GCE at scan rate 50 mVs^{-1} and pH=4.0

Electrode	E_{pc} (mV vs. Ag/AgCl)	E_{pa} (mV vs. Ag/AgCl)	$\lvert \Delta E_p \rvert$ (mV vs. Ag/AgCl)	$\lvert E_{pc}-E_{p/2} \rvert$ (mV vs. Ag/AgCl)	I_{pc} (μA)
SiW_{11}	−711	−664	47	35	−0.18
$SiW_{11}Co$	−714	−681	33	29	−0.18

E_{pc} cathodic peak potential, E_{pa} anodic peak potential, ΔE_p peak-to-peak separation, I_{pc} cathodic peak current, $E_{p/2}$ potential for $I=I_{pc}/2$

the transmitted beam and thence higher calculated absorbance values and surface coverages.

Cyclic voltammetry was also used to study the properties of the multilayer films in the presence of the negatively charged $[Fe(CN)_6]^{3-/4-}$ and the positively charged $[Ru(NH_3)_6]^{3+/2+}$ redox probes. Electrostatic attraction between the oppositely charged multilayer surface and the redox probe should improve the interfacial electron transfer process, whereas repulsion between identically charged multilayer surfaces and the redox probe would make the electron transfer reaction more difficult. Although many groups have used the $[Fe(CN)_6]^{3-/4-}$ redox couple to study the permeability of multilayer films [15, 35, 51–53], studies of electron transfer at films containing POMs are few.

Figure 4 shows cyclic voltammograms of $[Fe(CN)_6]^{3-/4-}$ at the electrode modified with $(PEI/SiW_{11}Co)_n$ for n=1, 2, 3 and 4. These results show that for an electrode coated with a single $(PEI/SiW_{11}Co)$ bilayer, the cyclic voltammogram exhibits quasi-reversible properties, indicating that the probe diffuses freely through the layer and undergoes electron transfer at the electrode surface. Increasing the number of multilayers from one to four leads to a decrease in peak currents and peak broadening and ultimately to an electrode with plateau-shaped current characteristics (Fig. 4). These observations show that an increased number of bilayers leads to a decrease in the number of hexacyanoferrate ions which reach the electrode substrate whenever the terminal layer consist of negatively charged $SiW_{11}Co$ anion. This is attributable to electrostatic repulsion of $[Fe(CN)_6]^{3-/4-}$ by the external negatively charged $SiW_{11}Co$ anion. When the outermost layer is the positively charged PEI the quasi-reversible properties in the cyclic voltammogram of $[Fe(CN)_6]^{3-/4-}$ are restored (data not shown), due to the electrostatic attraction of $[Fe(CN)_6]^{3-/4-}$ to the terminal positively charged PEI layer. The voltammogram is similar to that of a bare glassy carbon electrode, and is independent of film thickness (number of bilayers).

When the positively charged $[Ru(NH_3)_6]^{3+/2+}$ redox probe is used at the $(PEI/SiW_{11}Co)_n$ (n=1, 2, 3 and 4) modified electrode, the changes are not so significant (data not shown). The cyclic voltammograms for n=1 and 2 are equal, and increasing the number of multilayers from two to four leads to a slight decrease in the peak currents and to an increase in the peak-to-peak separation, when the POM is the outermost layer. However, after depositing a layer of PEI on the $(PEI/SiW_{11}Co)_1$ modified electrode (Fig. 5), the peak current due to $[Ru(NH_3)_6]^{3+/2+}$ decreases significantly and the peak-to-peak separation increases, owing to electrostatic repulsion of $[Ru(NH_3)_6]^{3+/2+}$ by the positively charged PEI.

The changes in peak current and peak-to-peak separation therefore indicate that electrostatic attractions or repulsions

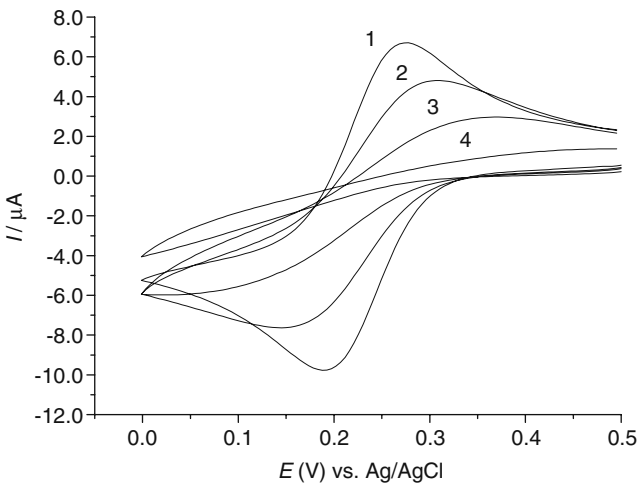

Fig. 4 Cyclic voltammograms of $[Fe(CN)_6]^{3-/4-}$ (1 mM, 1 M KCl) v=50 mVs^{-1}, at modified electrodes with $(PEI/SiW_{11}Co)_n$ for *1* n=1; *2* 2; *3* 3; and *4* 4

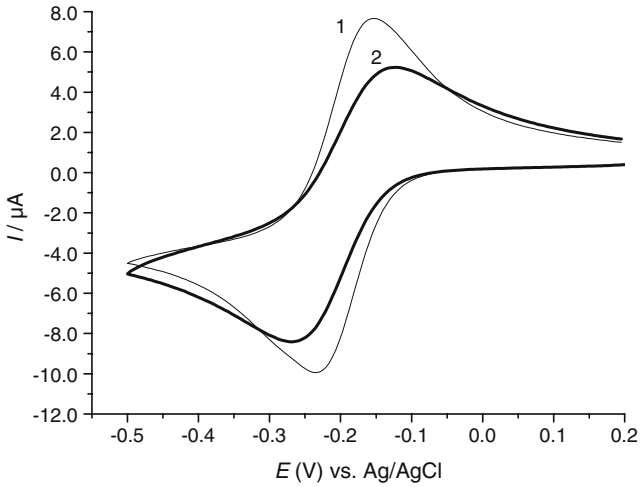

Fig. 5 Cyclic voltammograms of $[Ru(NH_3)_6]^{3+/2+}$ (1 mM, 1 M KCl) v = 50 mVs^{-1}, at modified electrodes with *1* $(PEI/SiW_{11}Co)_1$ and *2* $(PEI/SiW_{11}Co)_1/PEI$

have significant effects on the kinetics of the redox reactions, either accelerating or decelerating the processes.

To test the reproducibility of these LbL-modified electrodes, five electrode assemblies were prepared under identical conditions and the cyclic voltammograms recorded in $CH_3COOH/NaCH_3COO$ buffer solution (pH 4.0). The relative standard deviation of the peak current for the first tungsten reduction wave was 3.8% for $(PEI/SiW_{11}Co)_n$ and 4.6% for $(PEI/SiW_{11})_n$. Peak potentials did not change significantly. To test stability, modified electrodes were used during a whole day and kept overnight in their protecting case for 1, 3 or 8 days. No change in the shape and height of the redox waves was observed, as exemplified in Fig. 6 for the $(PEI/SiW_{11}Co)_7$ electrode.

Electrocatalytic effect of $(PEI/SiW_{11}Co)$ multilayer films on reduction of nitrite, bromate and iodate

An important application of electroactive LBL films is in electrocatalysis, since hybrid films can enhance the reduction/oxidation of many species that otherwise display sluggish electrochemical behaviour. Many studies have shown that reduced POMs are capable of delivering electrons to other species, thus serving as powerful electron reservoirs for multi-electron reduction [54–56]. In the studies reported here, the reduction of nitrite, bromate and iodate was used to test the electrocatalytic properties of $(PEI/SiW_{11}Co)_n$ multilayer films. Under the present experimental conditions, multilayer films of $(PEI/SiW_{11})_n$ did not show any electrocatalytic properties towards these compounds, as observed previously for this anion [23, 54].

Figure 7a presents cyclic voltammograms for the $(PEI/SiW_{11}Co)_7$ multilayer film modified electrode in the absence and in the presence of increasing concentrations

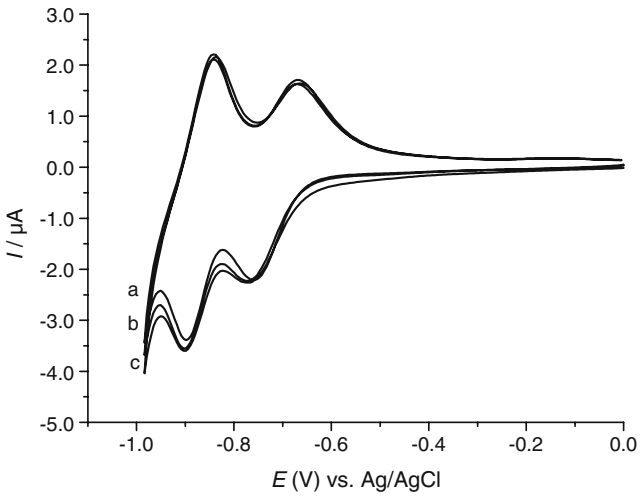

Fig. 6 Cyclic voltammograms for $(PEI/SiW_{11}Co)_7$ multilayer films in $CH_3COOH/NaCH_3COO$ buffer solution (pH 4.0), ν=25 mVs^{-1}: **a** first, **b** second, **c** eighth working day

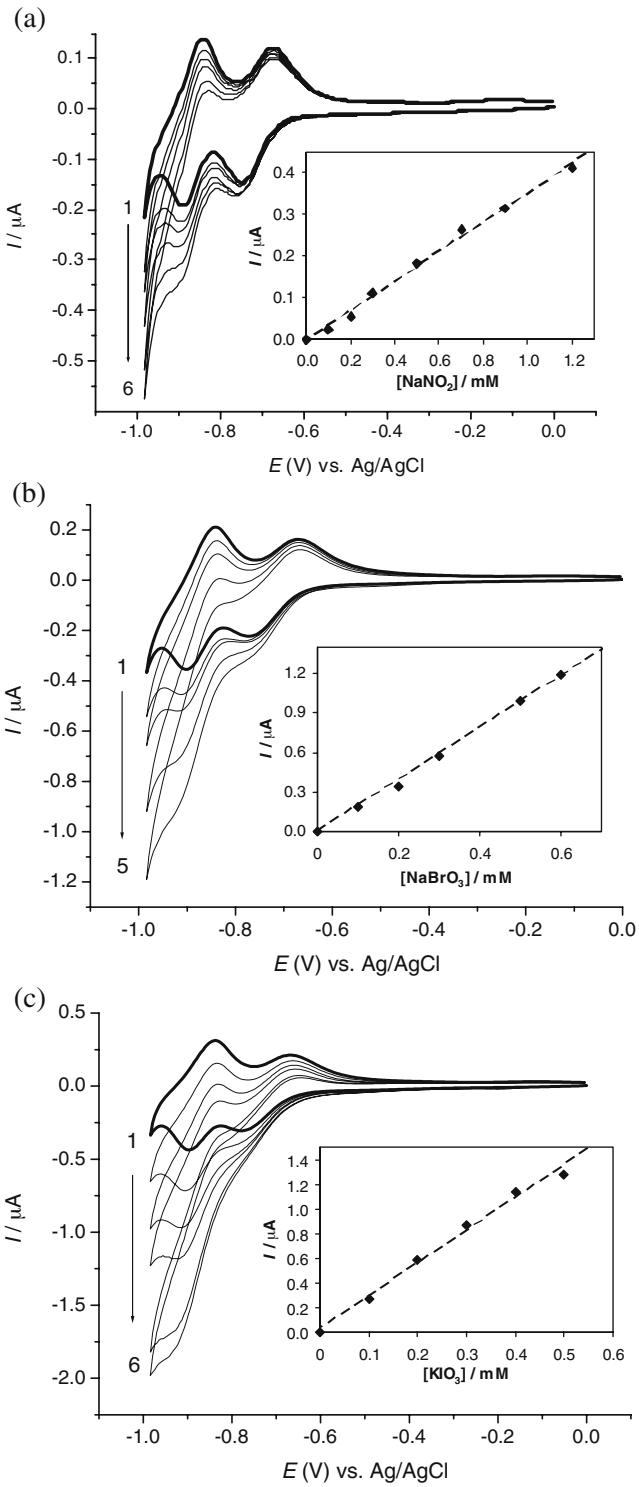

Fig. 7 Cyclic voltammograms of GCE/$(PEI/SiW_{11}Co)_7$ in pH 4.0 buffer solution obtained in the absence and in the presence of added concentrations of **a** nitrite: (1) 0; (2) 0.2; (3) 0.3; (4) 0.5; (5) 0.9 and (6) 1.2 mM, scan rate 25 mVs^{-1}, **b** bromate: (1) 0; (2) 0.1; (3) 0.3; (4) 0.6 and (5) 1.0 mM, scan rate 50 mVs^{-1}, **c** iodate: (1) 0; (2) 0.1; (3) 0.2; (4) 0.3; (5) 0.4 and (6) 0.5 mM, scan rate 50 mVs^{-1}. The *insets* show the catalytic peak current at −0.90 V vs. analyte concentration

of nitrite in the interval from 0 to 1.2 mM, at scan rate 25 mVs^{-1}. At pH 4.0, the second reduction wave of the $SiW_{11}Co$ anion at −0.9 V is significantly enhanced by the addition of nitrite, whereas the first is less affected. It is known that the electroreduction of nitrite/nitrous acid requires a large overpotential and that no response is observed at a CGE in a solution containing NO_2^- in the range of potentials used in this study [54]. The increase of peak current indicates that nitrite is being catalytically reduced at the modified electrode. The linear range for the catalytic current is up to a nitrite concentration of 1.2 mM, as shown in the inset, with a detection limit of 7.2×10^{-5} M, better than that obtained with a PMo_{12}-modified electrode (1×10^{-4} M) [57]. Additionally, these new modified electrodes allow higher concentrations of nitrite to be reached within the dynamic linear range than with electrodes modified with $SiW_{11}Fe$ than by other methodologies [23].

The results obtained for the reduction of bromate and iodate exhibit similar characteristics. As for nitrite, the wave associated with the first tungsten reduction is only slightly affected by the addition of bromate or iodate, but the peak current of the second tungsten reduction wave is significantly enhanced (Fig. 7b, c). The linear range for the catalytic current for bromate is up to 0.6 mM and for iodate is up to 0.5 mM, as shown in the insets. The detection limits were 3.7×10^{-5} and 5.8×10^{-5} M for bromate and iodate, respectively. These results indicate that the second cathodic wave has catalytic activity towards BrO_3^- and IO_3^-. The processes involved are [41]:

Electrochemical reactions:

$$SiW_{11}{}^{VI}Co(H_2O)O_{39}{}^{6-} + 2e^- + 2H^+ \rightarrow H_2SiW_2{}^{V}W_9{}^{VI}Co(H_2O)O_{39}{}^{6-} \quad (1)$$

$$H_2SiW_2{}^{V}W_9{}^{VI}Co(H_2O)O_{39}{}^{6-} + 2e^- + 2H^+ \rightarrow H_4SiW_4{}^{V}W_7{}^{VI}Co(H_2O)O_{39}{}^{6-} \quad (2)$$

Catalytic chemical steps:

$$3H_4SiW_4{}^{V}W_7{}^{VI}Co(H_2O)O_{39}{}^{6-} + BrO_3{}^- \rightarrow 3H_2SiW_2{}^{V}W_9{}^{VI}Co(H_2O)O_{39}{}^{6-} + Br^- + 3H_2O \quad (3)$$

$$3H_4SiW_4{}^{V}W_7{}^{VI}Co(H_2O)O_{39}{}^{6-} + IO_3{}^- \rightarrow 3H_2SiW_2{}^{V}W_9{}^{VI}Co(H_2O)O_{39}{}^{6-} + I^- + 3H_2O \quad (4)$$

Although the linear range of concentrations is not very high, the limits of detection are good, similar to that obtained for the detection of bromate with a $[SiNi(H_2O)W_{11}O_{39}]^{6-}$ modified electrode [39]. The main advantage of this $SiW_{11}Co$ modified electrode is that although this compound has already been used in other types of modified electrode, this is the first time that its catalytic activity has been demonstrated. Previous work with $SiW_{11}Co$ electrodes prepared by droplet evaporation methodology showed no catalytic activity towards nitrite [23].

Another important point for analytical applications is that after use as sensors in these electrocatalytic reactions, the electrodes could be totally recovered and regenerated, i.e. the original voltammograms could be restored, ready for further use.

Conclusions

It has been demonstrated that $(PEI/SiW_{11})_n$ and $(PEI/SiW_{11}Co)_n$ multilayer films can be successfully prepared on glassy carbon electrodes using layer-by-layer self-assembly and that the electrochemical properties of the two POMs are maintained. UV-vis spectroscopy demonstrated that the amount of POM adsorbed per deposition step is almost constant. The effect of scan rate in cyclic voltammetry shows that the tungsten reduction process is a surface-confined process and use of $[Fe(CN)_6]^{3-/4-}$ and $[Ru(NH_3)_6]^{3+/2+}$ electrochemical probes indicated that attractions or repulsions with the outermost layer have significant effects on kinetics of the redox reactions. With an increasing number of PEI/POM bilayers the peak currents of both redox probes gradually decreased, and the peak-to-peak separation increased, owing to kinetic and/or thermodynamic constraints associated with increase film thickness.

It was also shown that $(PEI/SiW_{11}Co)_n$ multilayer films exhibit electrocatalytic activity towards the reduction of nitrite, bromate and iodate with good dynamic linear ranges and detection limits.

Acknowledgments The authors thank the Fundação para a Ciência e a Tecnologia (FCT) for financial support (project POCI 2010-Feder-POCI/QUI/56534/2004). D. Fernandes acknowledges FCT for her PhD grant SFRH/BD/30797/2006. Thanks are also due to CICECO and the University of Aveiro.

References

1. Hill, CL (2007) Polyoxometalates in Catalysis. In: Hill CL (ed) J Mol Catal A Chem 262 (1–2): 2–6 (Thematic issue)
2. Hill CL, Prosser-McCartha CM (1995) Coord Chem Rev 143:407–455
3. Keita B, Nadjo L (2007) J Mol Catal A Chem 262:190–215
4. Rhule JT, Hill CL, Judd DA (1998) Chem Rev 98:327–357
5. Pope MT, Müller A (1991) Angew Chem Int Ed Engl 30:34–48
6. Gomez-Romero P (2001) Adv Mater 13:163–174
7. Coronado E, Giménez-Saiz C, Gómez-Garcia CJ (2005) Coord Chem Rev 249:1776–1796
8. Sadakane M, Steckhan E (1998) Chem Rev 98:219–237

9. Kozhevnikov IV (1998) Chem Rev 98:171–198
10. Coronado E, Mingotaud C (1999) Adv Mater 11:869–872
11. Polarz S, Smarsly B, Goltner C, Antonietti M (2000) Adv Mater 12:1503–1507
12. Keita B, Nadjo L (1988) J Electroanal Chem 243:87–103
13. Reybier K, Malugani JP, Fantini S, Herlem M, Fahys B (2002) J Electrochem Soc 149:E96–E101
14. Decher G (1997) Science 277:1232–1237
15. Liu S, Kurth DG, Bredenkotter B, Volkmer D (2002) J Am Chem Soc 124:12279–12287
16. Decher G (2003) In: Decher G, Schlenoff JB (eds) Multilayer thin films: sequential assembly of nanocomposite materials. Wiley-VCH, Weinheim
17. Kurth DG, Volkmer D, Klitzing RV (2003) In: Decher G, Schlenoff JB (eds) Multilayer thin films: sequential assembly of nanocomposite materials. Wiley-VCH, Weinheim
18. Qi W, Wu L (2009) Polym Int 58:1217–1227
19. Wang B, Vyas RN, Shaik S (2007) Langmuir 23:11120–11126
20. Bertrand P, Jonas A, Laschewsky A, Legras R (2000) Macromol Rapid Commun 21:319–348
21. Fernandes DM, Carapuça HM, Brett CMA, Cavaleiro AMV (2010) Thin Solid Films 518:5881–5888
22. Fernandes DM, Simões SMN, Carapuça HM, Brett CMA, Cavaleiro AMV (2010) J Electroanal Chem 639:83–87
23. Fernandes DM, Simões SMN, Carapuça HM, Cavaleiro AMV (2008) Electrochim Acta 53:6580–6588
24. Carapuça HM, Balula MS, Fonseca AP, Cavaleiro AMV (2006) J Solid State Electrochem 10:10–17
25. Wang Y, Guo C, Chen Y, Hu C, Yu W (2003) J Colloid Interface Sci 264:176–183
26. Ingersoll D, Kulesza PJ, Faulkner LR (1994) J Electrochem Soc 141:140–147
27. Cheng L, Pacey GE, Cox JA (2001) Electrochim Acta 46:4223–4228
28. Kulesza PJ, Chojak M, Miecznikowski K, Lewera A, Malik MA, Kuhn A (2002) Electrochem Commun 4:510–515
29. Liu J, Cheng L, Dong S (2002) Electroanal 14:569–574
30. Shiu K, Anson FC (1991) J Electroanal Chem 309:115–129
31. Gao S, Cao R, Li X (2006) Thin Solid Films 500:283–288
32. Triantis TM, Troupis A, Chassiotou I, Papaconstantinou E (2008) J Adv Oxid Technol 11:231–237
33. Li CX, Wang XG, Ma HY, Wang FP, Gu Y (2008) Electroanal 20:1110–1115
34. Ma H, Peng J, Han Z, Feng Y, Wang E (2004) Thin Solid Films 446:161–166
35. Gao S, Li T, Li X, Cao R (2006) Mater Lett 60:3622–3626
36. Cammack R, Joannou CL, Cui XY, Martinez CT, Maraj SR, Hughes MN (1999) Biochim Biophys Acta Bioenerg 1411:475–488
37. Khan N, Sultana S (2004) Toxicol 201:173–184
38. Kirisits MJ, Snoeyink VL, Inan H, Chee-Sandford JC, Raskin L, Brown JC (2001) Water Res 35:891–900
39. Chen CY, Song YH, Wang L (2009) Electrochim Acta 54:1607–1611
40. Cheng L, Liu J, Dong S (2000) Anal Chim Acta 417:133–142
41. Li Y, Bu W, Wu L, Sun C (2005) Sens Actuator B 107:921–928
42. Hamidi H, Shams E, Yadollahi B, Esfahani FK (2008) Talanta 74:909–914
43. Tourne CM, Tourne GF, Malik SA, Weakly TJR (1970) J Inorg Nucl Chem 32:3875–3890
44. Weakly TJR, Malik SA (1967) J Inorg Nucl Chem 29:2935–2944
45. Gamelas JAF, Cavaleiro AMV, Gomes EM, Belsley M, Herdtweck E (2002) Polyhedron 21:2537–2545
46. Nomiya K, Sugie Y, Amimoto K, Miwa M (1987) Polyhedron 6:519–524
47. Couto FARS, Cavaleiro AMV, de Jesus JD Pedrosa, Simão JEJ (1998) Inorg Chim Acta 281:225–228
48. Kuhn A, Anson FC (1996) Langmuir 12:5481–5488
49. Xu B, Xu L, Gao G, Guo W, Liu S (2009) J Colloid Interface Sci 330:408–414
50. Cheng L, Cox JA (2001) Electrochem Commun 3:285–289
51. Harris JJ, Bruening ML (2000) Langmuir 16:2006–2013
52. Pardo-Yissar V, Katz E, Lioubashevski O, Willner I (2001) Langmuir 17:1110–1118
53. Dai J, Jensen AW, Mohanty DK, Erndt J, Bruening ML (2001) Langmuir 17:931–937
54. Toth JE, Anson FC (1989) J Am Chem Soc 111:2444–2451
55. McCormac T, Fabre B, Bidan G (1997) J Electroanal Chem 427:155–159
56. Wang L, Xiao D, Wang E, Xu L (2005) J Colloid Interface Sci 285:435–442
57. Liang Y, He P, Ma Y, Zhou Y, Pei C, Li X (2009) Electrochem Commun 11:1018–1021